Journal of Molecular Liquids 444 (2026) 129173

Contents lists available at ScienceDirect

Journal of Molecular Liquids

journal homepage: www.elsevier.com/locate/molliq

Characterization of diluted mixtures of an ionic liquid in a hydrophobic natural deep eutectic solvent: Physicochemical, spectroscopic and electrochemical insights for its application in electrochemically controlled micro-extraction of heavy metals

Andrea Marco [a], César Quijada [b,*], Miguel Ángel Aguirre [a], Montserrat Hidalgo [a,*]

[a] Department of Analytical Chemistry, Nutrition and Food Science and University Institute of Materials (IUMA), University of Alicante, Spain
[b] Departamento de Ingeniería Textil y Papelera, Universitat Politècnica de València, Plaza Ferrándiz y Carbonell, 03801 Alcoy, (Alicante), Spain

ARTICLE INFO

Keywords:
Eutectic mixture
Transport properties
Cyclic voltammetry
Redox behavior
Sustainable separation process

ABSTRACT

In this work, a hydrophobic natural deep eutectic solvent (NADES) was made by mixing up DL-menthol and decanoic acid in a 2:1 molar ratio, and its mixtures with a soluble ionic liquid (1-hexyl-3-methylimidazolium chloride, [HMIM][Cl]) were investigated. A number of physicochemical properties (ionic conductivity, viscosity, and density) were either measured or estimated by the predictive UNIFAC model over a range of temperatures and [HMIM][Cl] compositions. The addition of [HMIM][Cl] enhances ionic conductivity, while keeping high fluidity and low density. However, Walden plots and dissociation degrees suggest that significant ion pairing occurs. The analysis of excess molar volumes and viscosity deviations suggests that the introduction of the IL up to 50 wt% gives rise to liquid structure with reorganization of the NADES hydrogen-bonding network. Such structural perturbation was confirmed by FT-IR measurements. The more diluted NADES + [HMIM][Cl] system showed an electrochemical stability window of about 2.5 V. Additionally, ferrocene/ferrocenium exhibits a quasi-reversible electron transfer with a standard rate of $(2.6 \pm 0.3)10^{-4}$ cm s^{-1} and a diffusion coefficient of $(6.16 \pm 0.06)\cdot10^{-8}$ cm^2 s^{-1}. To assess the viability of this medium in analytical applications, an electrochemically controlled liquid-liquid microextraction was conducted, employing the NADES+[HMIM][Cl] mixture as the extractant phase. This approach resulted in a notable enhancement (up to 8-fold gain vs the liquid-liquid microextraction in the absence of electric field) in the metal extraction efficiency from aqueous samples, underscoring the potential of the studied medium in both electrochemical and analytical applications.

1. Introduction

The search for sustainable, environmentally benign alternatives to the traditional volatile organic solvents (VOCs) has spurred significant interest in deep eutectic solvents (DESs) [1]. Their unique properties (eg. low vapor pressure, high thermal stability, high solvation power, wide electrochemical window, low toxicity, low cost and ease of preparation) have rendered these materials attractive as green alternatives to VOCs and conventional ILs for a broad spectrum of applications including (bio)catalysis, organic synthesis, biomass conversion, electrodeposition and electrochemical energy storage, extraction and separation processes, gas capturing and nanomaterials processing [2–5], as extensively investigated by Abbott's group and other leading research teams. Among the various subtypes of DESs, Type V hydrophobic DESs represent a relatively new category of eutectic solvents composed of non-ionic, molecular hydrogen bond acceptors (HBA) and donors (HBD) [6–8], which have been systematically explored by Marrucho's, Kroon's and Coutinho's groups. Formulated from naturally occurring compounds, terpene-based NADESs are paradigmatic examples of this subclass, combining renewable resources with hydrophobic characteristics that make them especially attractive for applications requiring water immiscibility. In this context, menthol-based NADESs, previously characterized in detail by Belikov and coworkers [9]—as those synthesized by combining menthol and decanoic acid (Men:Dec)—have been proposed as promising candidates for the extraction of analytes, like pollutants, drugs or value-added bioactive molecules [6,7,10], from aqueous media owing to their low viscosity and inherent hydrophobicity.

* Corresponding authors.
E-mail addresses: cquijada@txp.upv.es (C. Quijada), montserrat.hidalgo@ua.es (M. Hidalgo).

https://doi.org/10.1016/j.molliq.2025.129173
Received 28 August 2025; Received in revised form 16 December 2025; Accepted 18 December 2025
Available online 23 December 2025

In a previous work, Pinheiro et al. showed the excellent performance of a Men:Dec DES as the hydrophobic extractant phase in dispersive liquid-liquid microextraction (LLME) of elemental impurities in oral and parenteral drugs [11]. Over the last years, electrochemically controlled microextractions have emerged as an externally assisted variant of the conventional microextraction approach. This methodology is a physically stimulated extractive process where an applied electric field drives the migration of polar and ionic analytes into the extractant phase, either solid or liquid, significantly improving extraction efficiency and reducing operation times [12,13]. This approach has been effectively employed in solid- and liquid-phase microextraction to preconcentrate inorganic ions, drugs, or pollutants from various matrices, including water and wastewaters, foods and beverages or biological samples [12,14–16]. To the best of our knowledge, DESs have been utilized as a solvent media for the preparation of electroactive polypyrrole films as the sorbent phase in EC-solid phase microextraction by Asiabi et al. [17], but its direct use as a liquid extractant in EC-LLME has not been reported so far. Unfortunately, the non-ionic nature of neat Type-V NADESs results in limited or negligible ionic conductivity [18,19], which is a major challenge for their use in EC-LLME and more generally in electrochemical systems, where efficient charge transport is crucial.

To overcome this limitation, our research focused on mixing type V NADESs (i.e., menthol:decanoic acid (2:1)) with imidazolium-based ionic liquids, which are well known for their high ionic conductivity and electrochemical stability. Compared to mixtures of DES and water or polar and non-polar organic solvents [20–22], the number of reports dealing with the properties of DES-IL mixtures is very scarce. For example, Achsah et al. [23] studied the volumetric properties of mixtures of glyceline with butyl- and ethyl-imidazolium based-ILs at temperatures from 293.15 K to 343.15 K and Shekaari and coworkers [24] carried out a compatibility and thermodynamic study of low dilution mixtures of 1-ethyl-3-methylimidazolium ethyl sulfate with several choline-chloride-based DESs. These latter authors concluded that the IL has structure-breaking properties due to both the strength of hydrogen bonds formed between IL and DES and ion-dipole forces. In all these examples, the DESs are intrinsically ionic and show measurable conductivity even without any added IL, while Type V NADES-IL mixtures represent a fundamentally different conceptual framework where ionic conduction is provided by the IL in a non-conducting matrix. More recently, Panić et al. [25] prepared and thoroughly characterized a series of diluted mixtures of benzocainium ibuprofenate ILs in different menthol:decanoic acid DESs. These hybrid systems are conceptually similar to those described in this work, but the authors did not investigate ionic conductivity nor did they analyze ion transport mechanisms. Likewise, electrochemical properties of ionic DESs have been also extensively studied because of their current interest as sustainable solvents in metal processing [5], electroanalysis [26,27] and the development of power systems and battery technologies [4,28]. However, the analysis of non-ionic Type V DESs has received little attention. Recently, Chaabene et al. [19] carried out a detailed thermophysical and electrochemical study of a menthol-acetic acid DES with added ethanolamine as conductivity promoter. This novel solvent showed an electrochemical stability similar to that of hydrophilic ethaline and the redox probe hydroxymethylferrocene was proven to undergo a reversible and diffusion-limited charge transfer, with a diffusion coefficient of the same order of magnitude than those measured in ethaline and 1-ethyl-3-methylimidazoliumbis(trifluoro-methanesulfonyl) imide. Even more recently, Anjali and Pandey [18] demonstrated that the addition of ethanolamine to menthol/thymol:decanoic acid DESs causes significant microstructural changes leading to an anomalous increase in both viscosity and electrical conductivity.

In the present work a low toxicity IL, namely 1-hexyl-3-methylimidazolium chloride, [HMIM][Cl], was introduced into a Men:Dec (2:1) NADES matrix, in order to enhance its ionic conductivity while preserving its favorable hydrophobic character. Viscosity, density, conductivity and ion dissociation were systematically evaluated over a range of compositions and temperatures. These parameters are relevant for their practical significance for fluid dynamics, mass and ion transport, and they have a broad impact on many chemical, electrochemical and engineering processes (e.g., extractive operations). The electrochemical limits of stability of the solvent were determined by linear sweep voltammetry. Additionally, the electrochemical behavior was probed using cyclic voltammetry with ferrocene as a benchmark redox probe. The observed properties have favorable implications on its potential application in sustainable heavy metal extraction processes. This application was exemplified by using a dilute NADES-IL mixture as the hydrophobic extractant phase in EC-LLME operations from an aqueous sample, demonstrating improved extraction performance over a non-electro-assisted conventional LLME method.

Ultimately, this work lays a preliminary study for further exploration and practical implementation of hydrophobic Type-V NADES–IL systems in electrochemically driven extraction processes, offering a promising route toward greener analytical methodologies and environmental remediation strategies.

2. Experimental

2.1. Reagents

DL-Menthol (Men) and decanoic acid (Dec) were used as the HBA and HBD respectively in the synthesis of the hydrophobic Men:Dec NADES and 1-hexyl-3-methylimidazolium chloride ([HMIM][Cl] was used as conductivity promoter in the eutectic mixture. Ferrocene was employed as a benchmark redox probe for electrochemical studies.

Analytical reference solutions used for Inductively Coupled Plasma-Optical Emission Spectrometry (ICP-OES) calibrations were prepared by appropriate dilutions from a 1000 mg L^{-1} standard solution containing Cd, Cr, Ni, Pb, and Zn (High Purity Standards, Charleston, SC, USA) in HNO_3 medium. For enhancing the migration of the metals to the extractant phase, 8-hydroxyquinoline (8-HQ) dissolved in a mixture of acetic acid and ethanol absolute in volume ratio (1:4) was used.

All chemicals were used as received with no further purification. CAS numbers and purities as reported by the suppliers are listed in Table 1.

2.2. Synthesis of hydrophobic eutectic mixtures

The NADES was prepared by mixing Men and Dec with a molar ratio of 2:1 [11]. Proper amounts of each component were weighed with an analytical high-precision balance (SMG-215I-ION, VWR, Darmstadt, Germany) to an accuracy of ±0.01 mg. The mixture was stirred for 20 min at 60 °C to yield a homogeneous and colorless liquid. The prepared mixture was subsequently allowed to cool down to room temperature and stored in a tightly closed vial until further use.

Because of its inherent non-ionic nature, the Men:Dec NADES is a poor ionic conductor [18]. This property must be increased to make it feasible for the application of this eutectic mixture as a solvent for

Table 1
List of reagents (alphabetical order) and their relevant information as provided by the suppliers.

Reagent	CAS no	Supplier	Purity
Acetic acid	64–19-7	Sigma Aldrich	≥99.7 %
1-Hexyl-3-methylimidazolium chloride	171,058–17-6	IoLiTec (Heilbronn, Germany)	>98 %
Decanoic acid	334–48-5	Sigma-Aldrich	≥99.5 %
DL-Menthol	89–78-1	Sigma-Aldrich	≥95 %
Ethanol absolute	64–17-5	Sigma-Aldrich	≥99.5 %
Ferrocene	102–54-5	Sigma-Aldrich	98 %
8-Hydroxyquinoline	148–24-3	Sigma-Aldrich	> 99 %

electrochemical systems. To this end, addition of different common electrolyte organic salts (either directly or dissolved in polar and non-polar cosolvents) and mixing with a series of imidazolium-based ILs was attempted (see Supplementary material).

After this cursory study, [HMIM][Cl]-NADES mixtures resulted in a homogeneous and clear pale-yellow liquid, showing long term stability during storage and were prepared with the IL in proportions up to 50 wt %. Higher IL content resulted in mixtures progressively losing their hydrophobic character, becoming emulsified and eventually fully miscible with water at ca. ≥75 wt%, which made them unsuitable as the extractant phase in EC-LLME. Water content of freshly prepared neat compounds and their mixtures was determined in triplicate by using an automatic KF V20 Karl Fisher volumetric titrator (Mettler Toledo), with a limit of quantification of 100 ppm. The water contents of the IL-NADES mixtures were 0.18, 0.27, 0.31, 0.66 and 0.96 ± 0.01 wt%, for 10 wt%, 20 wt%, 25 wt%, 35 wt% and 50 wt% of added [HMIM][Cl], respectively. The mixtures contain more water than the neat NADES (0.04 wt %), but a lower amount than that reported for water-saturated Men:Dec DESs (> 2 wt%) [9,29]. Our own measurement for water-saturated 10 wt% IL-NADES gave 1.05 ± 0.01 wt% of water.

2.3. Ionic conductivity measurements

The specific conductivity of the eutectic mixtures was measured with an estimated accuracy of 1 % by using a CON 700 Conductivity Meter (Eutech Instruments, Dreieich, Germany) and a CONSEN9501D conductivity cell provided with stainless-steel ring electrodes (Eutech Instruments, Dreieich, Germany). All measurements were carried out by using a temperature-controlled water bath (J.P. Selecta, Barcelona, Spain). The temperature was accurate to ±0.1 K. The cell constant was determined with 5 μS cm^{-1}, 84 μS cm^{-1}, 1413 μS $cm^{-1}$and 12.88 mS cm^{-1} standard reference solutions (Mettler Toledo, Barcelona, Spain) at 25 °C. The temperature of the eutectic samples was allowed to equilibrate for 20 min before each conductance measurement.

2.4. Measurement and simulation of physicochemical properties

Kinematic viscosity was measured as a function of temperature in the range from 298.15 to 323.15 K by using a precalibrated Ubbelohde capillary viscometer, K = 0.1029 ± 0.0007 mm^2 s^{-2} (Comecta S.A., Barcelona, Spain). The viscometer was immersed in a recirculated water bath operated by a digital temperature controller XT5618B8 (XuTemp TempTech, Hangzhou, China) with a stability of ±0.02 K. The actual water bath temperature was monitored to an accuracy of ±0.2 K with a thermometer (EcoScan JKT) provided with a T-type thermocouple probe placed close to the capillary tube. Before each run, the viscometer was left to stand for thermal equilibrium at the desired temperature. Viscosities were obtained from the average flow times of three consecutive replicates. The flow time repeatability between individual runs was better than ±0.8 %. Kinematic viscosity values were then converted to dynamic viscosities by using simulated densities at the same temperatures.

Density was simulated using the software ASPEN PLUS® v12 with the UNIFAC predictive model. A brief account of the UNIFAC method and a list of the parameters used can be found in Table S6. Predicted dynamic viscosities were also obtained with the same methodology.

2.5. FT-IR characterization

FTIR measurements were carried out at an incidence angle of 45° using a Jasco 4700 FTIR spectrometer (Jasco Corporation, Tokyo, Japan), provided with a single reflection ATR accessory (ATR Pro One, equipped with a diamond crystal) and a DTGS detector. The spectra were the average of 16 scans recorded between 4000 and 600 cm^{-1} at room temperature and at a spectral resolution of 4 cm^{-1}.

2.6. Electrochemical characterization

All the electrochemical measurements were performed with a three-electrode cell using a PGSTAT101 Autolab Potentiostat from Metrohm (Herisau, Switzerland). A gold wire (purity >99.9 %, Sempsa JP) of 0.5 mm in diameter was used as the working electrode (WE) and a graphite plate of 3 cm^2 (isostatic graphite CGI-710, CGT Carbon GmbH) was employed as the counter electrode (CE). A silver wire was used as the pseudo reference electrode (RE). The working electrode was cleaned by thoroughly rinsing with acetone before each experiment. The electrochemically active surface area of the gold electrode was estimated to be 0.0296 cm^2 from the charge passed to build up a monolayer of chemisorbed oxygen in cyclic voltammetry (CV) experiments conducted in 0.5 M H_2SO_4 (see Fig. S1 for details) [30]. Linear sweep voltammetry was used to establish the electrochemical stability window (ESW) of 10 wt% IL-NADES. For its practical interest in electrochemically controlled liquid-liquid microextraction (EC-LLME) experiments, the stable potential window was also tested on a stainless-steel electrode made from a chromatography microliter syringe needle.

The behavior of the ferrocene/ferrocenium (Fc/Fc^+) redox probe dissolved in 10 wt% IL-NADES was studied by means of cyclic voltammetry (CV) on a gold wire electrode. Due to the low conductivity of the investigated media, the uncompensated resistance was of the order of 30 kΩ, as determined by electrochemical impedance measurements. Such high resistance cannot be automatically compensated for by the built-in positive feedback circuitry. Therefore, a manual point-by-point ohmic drop correction of each measured potential was performed. Before carrying out any electrochemical measurement, the solutions were deaerated by thorough bubbling of dry nitrogen, in order to remove dissolved oxygen. All the electrochemical experiments were performed under a dry nitrogen atmosphere to avoid the presence of oxygen and air moisture.

2.7. Applicability to liquid-liquid microextraction

In order to demonstrate the potential usability of the NADES as an extractive phase in electrochemical systems and its application to analytical science, the EC-LLME technique was employed for extracting traces of heavy metal ions from aqueous samples by using the 10 wt% [HMIM][Cl]-NADES eutectic mixture as the extractant phase.

The procedure, illustrated in Fig. 1, employed a chromatography microliter syringe (Hamilton, Bonaduz, Switzerland), with the plunger acting as the reference electrode and the stainless-steel needle as the working electrode. The plunger was previously silver-plated from an Ag^+ aqueous solution by electroless deposition with glucose as the reducing agent following a modification of the method proposed by Smith and coworkers [31]. The methodology entails the addition of the hydrophobic eutectic mixture (V = 315 μL) to the aqueous sample containing the metallic ion analytes and 1 % wt. v^{-1} 8-hidroxyquinoline as a chelating agent. The sample pH was adjusted to 4.66 with a sodium acetate/acetic acid buffer. The counter electrode was a graphite plate (isostatic graphite CGI-710, CGT Carbon GmbH) immersed in the aqueous sample phase. In a typical electrochemically driven extraction experiment, the working electrode was polarized at −0.75 V vs Ag for 5 min, while the sample was stirred with a magnetic stirrer (J.P. Selecta, Barcelona, Spain). After polarization, the recovered extract (V = 280 μL) was injected directly into the ICP-OES equipment. The experimental conditions and operational parameters described above were the result of a two-stage multivariate analysis (Plackett-Burman and central composite designs), and the details can be found elsewhere [32]. The optimized potential applied to the needle remained far from both the anodic and cathodic limits of stability of the extractant IL-NADES system.

The signal provided by the metal ions in the NADES phase after the microextraction procedure was determined by using an Agilent 5800 inductively coupled plasma optical emission spectrometer (Agilent

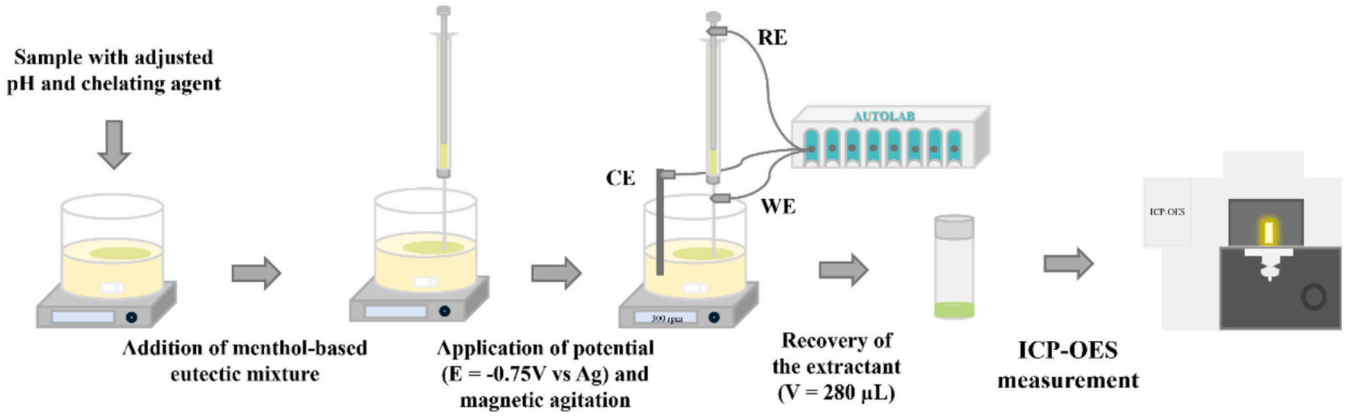

Fig. 1. Experimental procedure conducted to demonstrate the potential applicability of EC-LLME methodology employing menthol-based eutectic mixture as the extractant phase to enhance the extraction efficiency of metals in aqueous samples.

Technologies ICP-OES, Melbourne, Australia) operating in axial viewing mode. Argon (99.9992 %, Carburos Metálicos, Barcelona, Spain) was used in all measurements. Plasma operating conditions used in ICP-OES are shown in Table S7. The selected conditions provided the highest signal for the set of emission lines evaluated simultaneously.

To find out whether the extraction was more efficient or not than a conventional microextraction, the same experimental procedure was carried out in the absence of any electrical field.

3. Results and discussion

3.1. Physicochemical characterization

All the physicochemical properties studied were measured and/or simulated as a function of temperature (in the range from 298.15 to 323.15 K) at atmospheric pressure.

3.1.1. Transport and volumetric properties

Fig. 2a shows the temperature dependence for the specific ionic conductivity, κ, of the neat [HMIM][Cl] (data from ref. [33]) and its mixtures with Men:Dec (2:1) at different compositions. Detailed conductivity data and their experimental uncertainties can be found in Table S8. The neat NADES exhibits negligible conductivity across the studied range (see Table S8), indicating strong HBA-HBD hydrogen bonding that prevents the release of free protons. In contrast, even moderate additions of [HMIM][Cl] significantly enhance conductivity, with a pronounced jump between 35 and 50 wt% IL. This gap likely arises from residual water (~1 wt% in the most concentrated mixture), which is known to promote ion mobility. In fact, conductivity increased from 7.17 µS cm^{-1} to 9.29 µS cm^{-1} upon water saturation of a 10 wt% IL mixture at 25 °C. At a constant IL concentration, the conductivity increases with the rising temperature, as usually observed for electrolyte solutions [34], ILs [35] and ionic DESs [22,36]. This behavior results

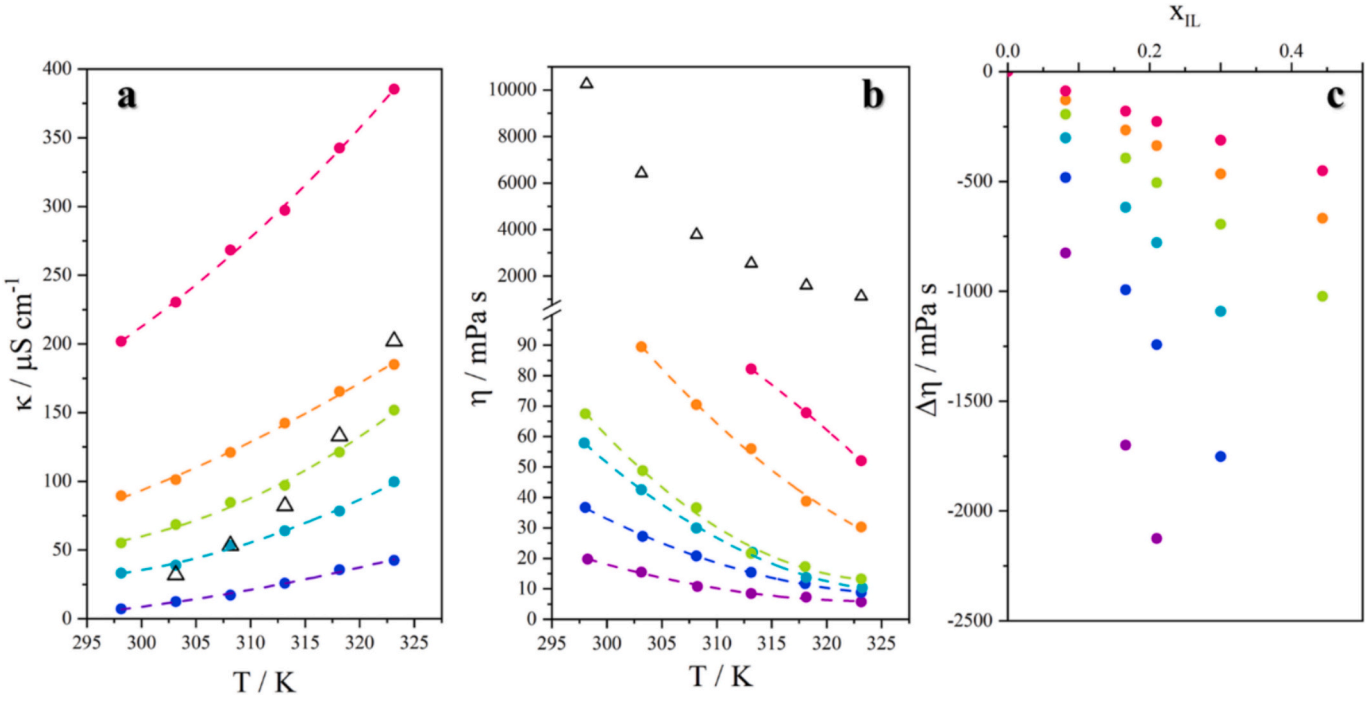

Fig. 2. Temperature dependence of measured (a) ionic conductivity, (b) viscosity and (c) viscosity deviation of Men:Dec (2:1) NADES + [HMIM][Cl]) liquid mixtures; w_{IL}: 0 wt% (purple circles); 10 wt% (blue circles); 20 wt% (light blue circles); 25 wt% (green circles); 35 wt% (orange circles); 50 wt%.(pink circles). Conductivities and viscosities for pure [HMIM][Cl] from Ning et al. [33] (black open triangles). Dashed lines correspond to regressed Arrhenius-like curves (see text). (For interpretation of the references to colour in this figure legend, the reader is referred to the web version of this article.)

from lowering the viscosity of the liquid mixture upon heating. While the pure [HMIM][Cl] is less conductive than the 50 wt% IL-NADES mixture, its conductivity curve crosses those for mixtures containing 20–35 wt% IL This behavior reflects the complex interplay of solution viscosity, ion mobility, ion pairing and other association phenomena that govern charge transport.

Fig. 2b shows the temperature dependence of the experimental dynamic viscosity of the neat NADES and its mixtures (see Table S9). Literature viscosity values for pure [HMIM][Cl] [37] are also shown for comparison (open symbols). Dynamic viscosities were obtained from measured kinematic viscosities using densities estimated with the UNIFAC model (Table S11). The simulated densities for the neat NADES at 298 K matched well the value reported by Van Osch and coworkers (899.51 kg m^{-3}) [29] and our own measurement carried out by picnometry at 295 K (897.35 kg m^{-3}). At the same temperature, the model also accurately reproduces the measured density of the 10 wt% IL-NADES mixture (910.29 kg m^{-3}) within 0.1 %. In addition, our results deviate by only +0.19 % from the experimental density values reported for pure L-Men:Dec [10]. Dynamic viscosities predicted with UNIFAC (Table S10) also exhibit very good agreement with experimental measurements.

Water impurities are known to affect density and viscosity of DES, but literature reports only minor deviations (~0–5 %) even at water contents above 2 wt% in Men:Dec 2:1 [29,38]. Our own viscosity measurements on a water-saturated 10 wt% IL-NADES show a modest decrease of ca. 2.7 % at 298 K, well within the experimental error (3.3 %, Table S9). Therefore, the low water levels in our mixtures are not expected to modify significantly the reported properties.

Both density and viscosity of the mixtures increase with IL addition due to the higher density and viscosity of [HMIM][Cl]. As typically found in liquids such as electrolyte solutions, molten salts, ILs and DES, both properties decrease with the increasing temperature because thermal motion weakens hydrogen bonding and increases the available free volume. Linear regression of density and the calculated isobaric thermal expansion coefficients can be found in the Supplementary material (Fig. S2, Tables S12–13).

The excess molar volume, V_m^E, $cm^3 \cdot mol^{-1}$,(Eq. 1), was obtained according to the expression:

$$V_m^E = \sum_{i=1}^{2} x_i M_i \left(\frac{1}{\rho} - \frac{1}{\rho_i}\right) \quad (1)$$

where ρ (g cm^{-3}) and ρ_i (g cm^{-3}) stand for the density of the mixture and of the pure component *i*, respectively, while x_i and M_i refer to the mole fraction and molar mass ($g \cdot mol^{-1}$) of the mixture components. One should note that we treated these liquid systems as binary mixtures, with the molar mass of the NADES being calculated as a composition-weighted average ($M_{DES} = 2/3M_{Men} + 1/3M_{Dec}$) [22].

The excess molar volume is positive for all the compositions and temperatures studied (Table S14) and increases with both IL mole fraction and temperature (Fig. S3). The sign of V_m^E indicates a less efficiently packed structure than expected for ideal behavior. The reorganized structure can be explained by weaker intermolecular interactions and/or impaired interstitial accommodation of solute IL within the NADES hydrogen-bonding network [39,40]. Partial dissociation of the IL into discrete ions and partial breaking and reorganization of the DES structure may contribute to these effects. The average hole radii (ca. 0.20 nm, as calculated from predicted surface tension values) suggest that free voids can host small chloride ions (0.18 nm, [35]), but not the larger hexyl-methylimidazolium cations (ca. 0.35 nm, [35]). Positive deviations contrast with volume contraction commonly observed when alkylimidazolium-based ILs or DES are diluted in polar solvents [21,22,39,41–43], where effective and strong coordination of solute by solvent molecules and dense packing dominate.

Viscosity deviations, (Eq. 2), were calculated by using the linear mixing rule to account for the ideal viscosity of the mixtures:

$$\Delta\eta = \eta - \sum_i x_i \eta_i \quad (2)$$

With η (mPa s), η_i (mPa s) and x_i referring to as the measured viscosity of the mixture, the viscosity of the pure components and the mole fraction of the mixture components, respectively. Fig. 2c shows the temperature dependence of Δη for the different IL-NADES mixtures at different IL concentrations (cf. Table S15). Viscosity deviations are negative throughout the studied range and become more negative with the increasing IL mole fraction, while their magnitude decreases with temperature. This trend has been found in mixtures of imidazolium-based ILs [39,42,43] and choline chloride-based DES diluted in non-aqueous solvents [21]. The observed pattern is also consistent with structural reorganization of the solvent, reduced Coulomb interactions between IL ions, and weaker solute-solvent interactions, which results in faster molecular motions relative to ideal mixtures [40]. Lower viscosity deviations at higher temperatures suggest that NADES hydrogen-bonding interactions and IL ion-ion interactions weaken more rapidly with temperature than IL-NADES interactions do [21].

3.1.2. Energy and thermodynamics of activation

Arrhenius plots of ionic conductivity and viscosity of the neat NADES and its mixtures with [HMIM][Cl] are shown in Fig. S5. Although the Vogel-Fulcher-Tamman (VFT) equation is often preferred for ILs and DESs (particularly over broad temperature ranges approaching the glass-transition region), in our narrower interval we found that the Arrhenius model (Eq. 3) [5] provided general better adherence, yielding lower standard deviations and average relative deviations.

$$Y = A_Y \exp\left(\frac{B_Y}{RT}\right) \quad (3)$$

This expression relates the property *Y* (κ or η) to the pre-exponential factor A_Y and the parameter B_Y which corresponds to the activation energy for ionic transport ($-E_{a,\kappa}$) or the viscous flow ($E_{a,\eta}$). Fitting parameters obtained from the Arrhenius correlations are shown in Table 2, jointly with the R-squared coefficient and standard errors. The activation energy for viscous flow increases with IL content, reaches a maximum, and then decreases, whereas the activation energy for conductivity decreases monotonically Except for the most diluted solution, $E_{a,\eta}$ largely exceeds $E_{a,\kappa}$, which seems typical of [HMIM][Cl]-based systems [33]. In the 10 wt% eutectic mixture $E_{a,\eta}$ is unusually lower than $E_{a,\kappa}$, indicating that viscous flow is energetically easier than ionic motion.

The relationship between kinematic viscosity, ν, and transition-state thermodynamic properties was analyzed through the Eyring' theory of absolute reaction rates, according to Eq. 4 [19]:

$$\nu = \frac{hN_A}{M} \exp\left(-\frac{\Delta S^{\ddagger}}{R}\right) \exp\left(\frac{\Delta H^{\ddagger}}{RT}\right) \quad (4)$$

where $\Delta H^{\ddagger}$ and $\Delta S^{\ddagger}$ are the enthalpy and entropy of activation, *M* is the composition-weighted average molar mass of the mixed eutectic liquid, *h* is the Planck's constant, N_A is the Avogadro's number and *R* is the universal gas constant. Following the procedure by Chaabene et al. [19],

Table 2
Energies of activation of ion transport and viscous flow for Men:Dec (2:1) NADES + [HMIM][Cl] liquid mixtures.

w_{IL} (wt%)	$E_{a,\kappa}$ (kJ mol^{-1})	R^2	$E_{a,\eta}$ (kJ mol^{-1})	R^2	$E_{a,\kappa}/E_{a,\eta}$
0	n/a		40.2 ± 1.9	0.991	
10	57 ± 4	0.984	45.6 ± 0.5	0.9995	1.25
20	35.5 ± 1.4	0.994	56 ± 2	0.993	0.64
25	31.7 ± 1.1	0.995	58 ± 4	0.989	0.59
35	24.2 ± 0.7	0.997	45 ± 2	0.990	0.53
50	20.7 ± 0.4	0.999	38 ± 4	0.995	0.54

plots of $\ln\left(\frac{\nu M}{hN_A}\right)$ vs. T^{-1} (Fig. S6) were used to obtain $\Delta H^{\ddagger}$ and $\Delta S^{\ddagger}$, which are listed in Table 3 together with regression statistics. As noted previously [19], the activation energy for the viscous flow is dominated by the enthalpic term, i.e. $E_{a,\eta} \approx \Delta H^{\ddagger}$.

3.1.3. Walden plots

The large differences between the activation energies for ionic conduction and viscous flow suggest that charge transport in the IL-NADES mixtures is not fully ionic, and deviations from the empirical Walden rule ($\Lambda_m \eta = C$, where Λ_m is the molar conductivity and C is a constant characteristic of the free solvated ions) should be expected [44,45]. The fractional Walden rule ($\Lambda_m \eta^{\alpha} = C$, $0 < \alpha \leq 1$), commonly used for molten salts, ILs [33,44–46] and ionic DES [36,47] was therefore applied. Fig. 3 shows the Walden plots (log Λ_m vs. log (1/η)) for the various IL-NADES liquid mixtures at different temperatures. Since viscosity measurements exhibited a slight offset between the thermostat setpoint and the actual temperature, viscosities were interpolated to the exact conductivity measurement temperatures using the Arrhenius fits. The molar conductivity, Λ_m (S cm^2 mol^{-1}) was calculated from the specific conductivity, (κ, S cm^{-1}) by using the mixture density (ρ, g cm^{-3}), the IL mass fraction, w_{IL} and the molar mass of the IL (M_{IL}, g mol^{-1}) according to Eq. 6:

$$\Lambda_m = \frac{\kappa}{c_{IL}} = \frac{\kappa}{w_{IL}} \frac{M_{IL}}{\rho} \tag{6}$$

The resulting Walden plots (Fig. 3) show good linearity and the fitting parameters (slope α and y-intercept log C) are listed in Table 4. Unlike [HMIM][Cl] and other dialkylimidazolium ILs, or standard DESs such as ethaline (open squares), the IL-NADES liquid mixtures lie well below the 0.01 M KCl reference line (α = 1), indicating subionic liquid behavior, with very low Angell's ionicity [45]. Interestingly, this behavior resembles that of other menthol-based DES such as menthol: acetic acid:ethanolamine [19] (Fig. 3, open triangle). The observed slopes deviate markedly from unity and closely correlate with the ratio $E_{a,\kappa}/E_{a,\eta}$ (Table 2), in line with earlier observations by Schreiner and coworkers for fluoroborate-based ILs [44].

The significant deviations from the ideal Walden rule confirm that the IL is not fully dissociated into free ions, but it may form ion pairs or larger aggregates. Even at low IL content, ion association is likely to be favored by inefficient screening of coulombic attractions in the low permittivity NADES (ε = 3.845) [10] and by H-bonding forces between IL counterions [48]. Similar prevalence of ion pairs has been reported in mixtures such as [BMIM][BF_4]/dichloromethane, [HMIM][Tf_2N]/chloroform and [EMIM][Tf_2N]/chloroform at $x_{IL} \leq 0.01$ [49,50].

Remarkably, the fitted log C values approach the ideal Walden y-intercept as the IL concentration increases, indicating higher ionicity and ion dissociation. This trend is the opposite of that for classic electrolyte solutions in high relative permittivity solvents, where dissociation rises upon dilution. Instead, this behavior matches observations for ILs dissolved in low-dielectric molecular solvents, in which "re-dissociation" of neutral ion pairs into charged ion triplets or larger ion aggregates [48,49]. This increase in mobile charge carriers explains the rise in molar conductivity with IL content (Table S16), consistent with our experimental observations.

Table 3
Activation thermodynamic functions of viscous flow for Men:Dec (2:1) NADES + [HMIM][Cl] liquid mixtures.

w_{IL} (wt%)	ΔH‡ (kJ mol^{-1})	ΔS‡ (J K^{-1} mol^{-1})	R^2
0	39.5 ± 1.9	57 ± 6	0.991
10	44.9 ± 0.5	69.7 ± 1.6	0.9990
20	55 ± 2	100 ± 8	0.993
25	53 ± 3	93 ± 9	0.989
35	44 ± 2	57 ± 8	0.990
50	39 ± 4	35 ± 11	0.992

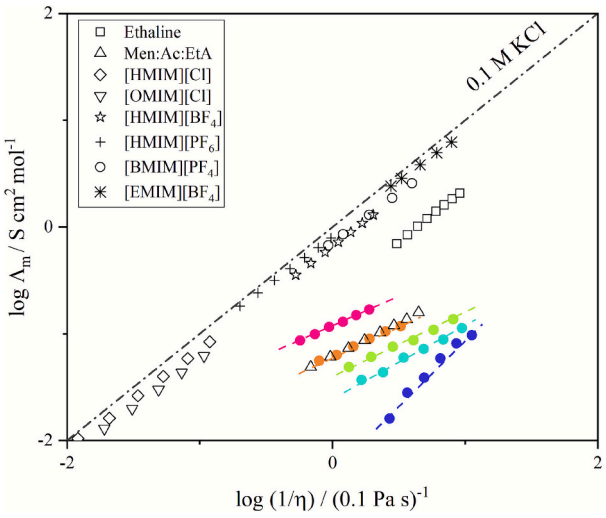

Fig. 3. Walden plots for Men:Dec (2:1) NADES + [HMIM][Cl]) liquid mixtures at different temperatures; w_{IL}: 10 wt% (blue circles); 20 wt% (light blue circles); 25 wt% (green circles); 35 wt% (orange circles); and 50 wt% (pink circles).Open symbols are referred to literature values for different DES and ILs [19,33]. The dashed line corresponds to the ideal Walden line, taken from a reference 0.01 M KCl aqueous solution. (For interpretation of the references to colour in this figure legend, the reader is referred to the web version of this article.)

Table 4
Linear fitting parameters for fractional Walden plots of Men:Dec (2:1) NADES + [HMIM][Cl] eutectic mixtures.

w_{IL} (wt%)	α	Log (C/S cm^2 mol^{-1})	R^2
10	1.27 ± 0.08	−2.297 ± 0.062	0.984
20	0.648 ± 0.024	−1.588 ± 0.016	0.994
25	0.557 ± 0.019	−1.382 ± 0.011	0.996
35	0.548 ± 0.014	−1.205 ± 0.004	0.997
50	0.556 ± 0.010	−0.9280 ± 0.0018	0.998

3.1.4. Ion dissociation

The degree of ion dissociation, ξ, is typically estimated from the ratio of experimentally observed conductivity to that predicted theoretically by the Nernst–Einstein equation (Eqs. 7 and 8). In these expressions, c_i stands for the concentration of ion i, z_i is its charge and D_i its diffusion coefficient, while F corresponds to the Faraday constant:

$$\xi = \frac{\kappa}{\kappa_{NE}} \tag{7}$$

$$\kappa_{NE} = \sum_i \frac{F^2 c_i z_i^2 D_i}{RT} \tag{8}$$

Nordness et al. [48,51] showed that ion dissociation can be estimated to a reasonable accuracy by relating diffusion coefficients to viscosity through the Stokes-Einstein relation (Eq. 9), where $r_i$is the effective ionic radius and $C$is a constant ranging from 6π (stick boundary) to 4π (slip boundary) [51,52].

$$D_i = \frac{RT}{N_A C r_i \eta} \tag{9}$$

For a symmetric univalent IL, combining and rearranging Eqs. 7–9, and expressing composition in terms of mass fraction leads to Eq. 10, which enables ξ to be estimated with reasonable accuracy from experimental conductivity and viscosity [48,51], provided that reliable ionic radii are available [53,54].

$$\xi = \frac{\kappa C N_A M_{IL} \nu}{F^2 w_{IL} \sum_i (1/r_i)} \tag{10}$$

In this work, we used a modified version of the Nordness method by substituting Eyring's viscosity expression (Eq. 4) into Eq. 10. This yields Eq. 11, which relates the dissociation degree explicitly to conductivity and temperature, enabling the calculation of ξ values using the activation enthalpy and entropy associated with viscous flow (Table 3):

$$\xi = \frac{\kappa C N_A^2 h M_{IL}}{F^2 w_{IL} M \sum_i (1/r_i)} \exp\left(-\frac{\Delta S^{\ddagger}}{R}\right) \exp\left(\frac{\Delta H^{\ddagger}}{RT}\right) \tag{11}$$

Using this formulation, ξ values for [HMIM][Cl] dissolved in Men:Dec (2:1) were calculated at different compositions from experimental conductivity values between 298.15 and 323.15 K and compared with those reported in the literature for solutions of ILs in conventional solvents (Fig. 4). The slip condition (C = 4π) was deemed more appropriate because it applies to diffusing solute particles that interact weakly with surrounding solvent molecules and for solute-solvent pairs of comparable size [50,53]. Two limiting scenarios were examined for comparison: (i) dissociation of the IL into free cations $[C]^+$and anions $[A]^-$, and (ii) the additional formation of charged ion triplets $[ACA]^-$and $[CAC]^+$arising from the reorganization of neutral ion pairs. Effective radii of free ions were taken as the Van der Waals values reported by Tokuda et al. ($r_+ = 0.353$ nm, $r_- = 0.181$ nm [53,55]), and ion triplets radii estimated from their sum.

According to our estimations, the dissociation of [HMIM][Cl] into free ions is low ($\xi \leq 0.15$) across the composition range $0.08 < x_{IL} < 0.44$ (Fig. 4a). When ion-triplet formation is considered, ξ values increase markedly (Fig. 4b). In both scenarios, ion dissociation increases monotonically with IL content and decreases slightly with temperature, in agreement with literature trends [48]. The composition dependence contrasts with the U-shaped profiles typically observed for alkyl imidazolium- or alkyl-piperidinium-based ILs dissolved in aqueous and polar organic solvents, where dissociation decreases to a minimum before rising at extreme dilution [48,51]. Instead, our results show good qualitative agreement with ion dissociation patterns reported for dialkyl-imidazolium-based ILs containing $[BF_4]^-$, $[PF_6]^-$ or $[Tf_2N]^-$ dissolved in low permittivity solvents (ε ~ 9–5) [48,56]. The agreement is even stronger when ion-triplet species are considered, which is expected according to the extremely low dielectric constant of the NADES (ε = 3.845) [10] and the strong electrostatic interactions between $[HMIM]^+$ and Cl^-, given the high charge density of the chloride anion compared to much larger $[BF_4]^-$ or $[Tf_2N]^-$ [54]. Under such conditions, free ions are expected to exist only at very low concentrations, while ion-paired or aggregated species are favored at higher IL contents. Accordingly, actual ξ values likely lie between the limiting scenarios considered may shift from the free-ion dominated behavior at very low IL content toward ion-triplet–dominated behavior as the IL fraction increases. Regardless of the uncertainties in absolute ξ values, our estimate provides valuable qualitative trends consistent with the deviations from Walden behavior and with the observed increase in molar conductivity as IL concentration rises.

3.2. Spectroscopic characterization

FT-IR spectroscopy was employed to examine changes in the chemical structure and intermolecular interactions in the Men:Dec NADES upon increasing additions of [HMIM][Cl]. Fig. 5 displays stacked spectra of mixtures containing 10–25 wt% IL, together with the spectra of the neat NADES (bottom) and IL (top) for reference.

The NADES spectrum exhibits the characteristic O—H stretching band of DL-menthol (3378 cm^{-1}) and the carbonyl stretch of decanoic acid (1709 cm^{-1}), confirming hydrogen-bond formation between the menthol hydroxyl group and the acid carboxyl group [6,57]. Other characteristic absorption peaks of both components remain unchanged: C—H stretching (2953 cm^{-1}, 2921 cm^{-1} and 2853 cm^{-1}), C—H bending (1455 cm^{-1} and 1368 cm^{-1}) and C—O stretching bands (1079 cm^{-1} and 1043 cm^{-1}) [57]. The neat IL shows imidazolium ring vibrations in the 1600–600 cm^{-1} region [58], and aliphatic stretching bands of the hexyl chain between 3000 and 2800 cm^{-1} [58,59]. The bands assigned to higher-frequency C_2—H and $C_{4,5}$–H stretching modes of imidazolium (3042 and 3136 cm^{-1}) are highly sensitive to cation–anion hydrogen bonding [58,59]. A broad band at ~3380 cm^{-1} arises from trace water.

In IL–NADES binary mixtures, the 1600–600 cm^{-1} region is dominated by NADES absorption features, while imidazolium ring bands (1567, 1168, 654 and 623 cm^{-1}) progressively increase in intensity with IL concentration. The positions and shapes of these bands, as well as those of the aliphatic C—H stretching region, remain essentially unaltered, indicating preservation of the chemical structure of the HBD, HBA, and IL cation. The invariance of the 1567 cm^{-1} band rules out

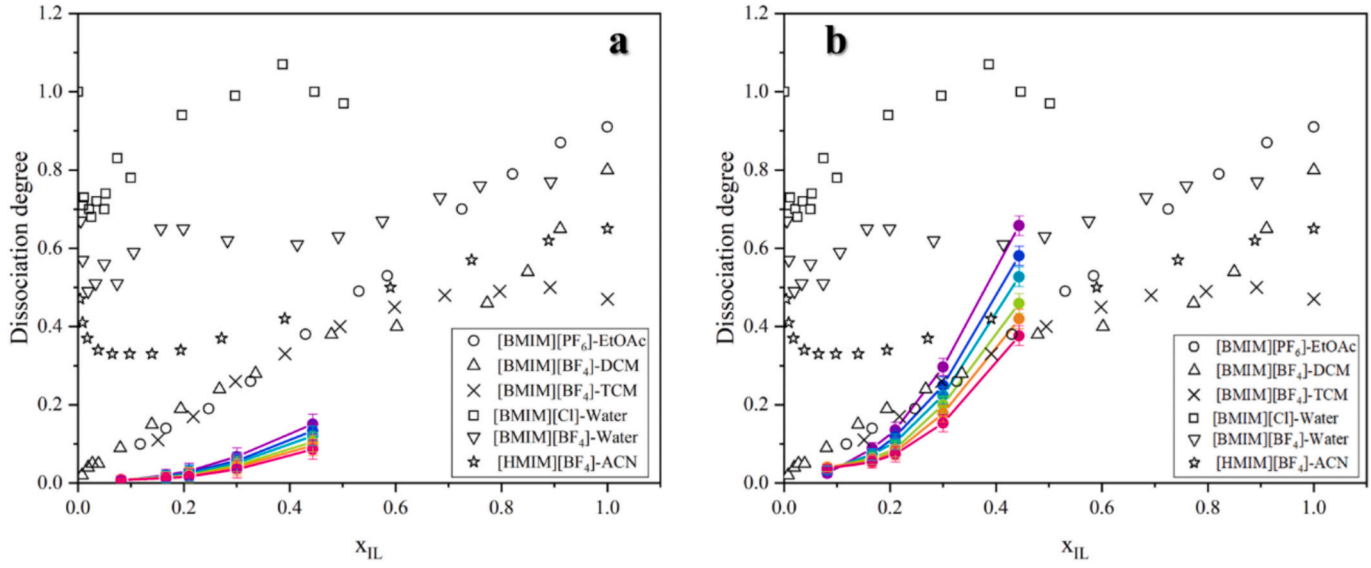

Fig. 4. Calculated dissociation degrees of IL in Men:Dec (2:1) NADES + [HMIM][Cl] eutectic mixtures as a function of composition and temperature; a) only discrete ions; and b) including ion triplets. T: 298.15 K (purple circles);303.15 K (blue circles); 308.15 K (light blue circles); 313.15 K (green circles); 318.15 K (orange circles); and 323.15 K (pink circles). Open symbols correspond to data compiled in ref. [48]. (For interpretation of the references to colour in this figure legend, the reader is referred to the web version of this article.)

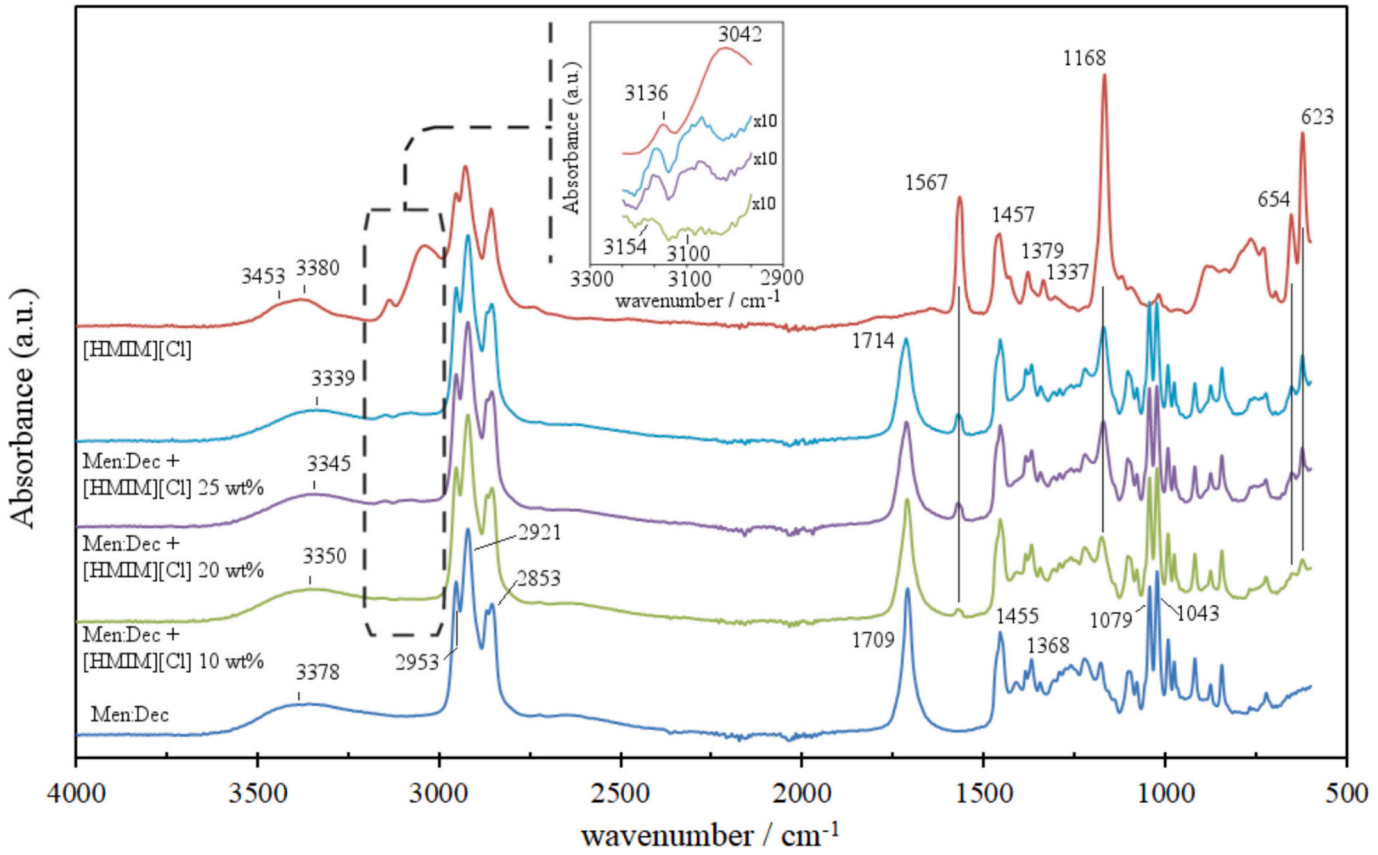

Fig. 5. FT-IR spectra of neat [HMIM][Cl] (top), neat Men:Dec 2:1 (bottom) and their mixtures.

significant π–dipole interactions between the imidazolium ring and NADES components.

The vibrational modes most sensitive to hydrogen bonding exhibit systematic and composition-dependent changes. Increasing IL content induces a red shift of the menthol O—H stretching band (3378 to 3339 cm^{-1}) and a slight broadening and blue shift of the decanoic acid C═O stretch (1709 to 1714 cm^{-1}). Peak deconvolution (Figs. S6-S7) reveals that the O—H band remains a single broad feature, whereas the C═O band splits into two contributions, with a new component at 1720–1730 cm^{-1} whose intensity increases with IL concentration. These spectral evolutions suggest a redistribution of hydrogen bonds involving weakening of menthol–acid interactions and formation of IL-associated carboxyl species, likely mediated by chloride acting as a proton acceptor. Proton donation from menthol to chloride, leading to strong O–H···Cl^- interactions, may also contribute to the observed O—H red shift. Similar chloride-driven reorganizations have been reported for alkyl-imidazolium chloride- and ethylpyridinium chloride-based DESs formed with amide, lactam, and carboxylic-acid HBDs [60,61]. In parallel, the imidazolium C—H stretching modes undergo substantial blue shifts (20–50 cm^{-1}) upon dilution, thereby pointing to a weakening of C_2–H···Cl^- and $C_{4,5}$–H···Cl^- hydrogen bonds and, consequently, reduced cation–anion interaction strength in the IL. This destabilization is consistent with competitive hydrogen bonding between chloride and NADES donors, as also observed in bezocainium ibuprofenate IL mixed with Men:Dec DESs [25].

Our spectroscopic results are consistent with the macroscopic transport-property trends and support the idea that addition of [HMIM][Cl] perturbs the NADES hydrogen-bond network, leading to a less compact liquid structure. Although the present data highlight the dominant role of hydrogen-bond reorganization, additional solute–solvent interactions (e.g., ion–dipole forces, π–π interactions, or dispersion contributions) may also participate in the structural modification. Further spectroscopic and computational studies will be required to elucidate their specific roles.

3.3. Electrochemical properties

According to the physicochemical characterization described above, the most diluted [HMIM][Cl]–Men:Dec (2:1) eutectic mixture behaves as a hydrophobic liquid with relatively low viscosity and density, and with sufficient, although modest, ionic conductivity owing to partial dissociation of the IL. These properties make the 10 wt% [HMIM][Cl] mixture an attractive, low-toxicity medium for electrochemically driven extraction processes. Therefore, the electrochemical study presented in this section focuses on this composition.

3.3.1. Potential window of electrochemical stability

Before considering any practical electrochemical application for a new electrolyte/solvent system, it is crucial to define its ESW. Fig. 6 shows the ESW of the 10 wt% IL-NADES system on gold and stainless-steel wire electrodes measured using linear sweep voltammetry (LSV) at a sweep rate of 20 mV s^{-1}. The ESW limits were established by taking a cutoff current density of ±1.0 mA cm^{-2} [5].

The stability window (~2.5 V) is significantly narrower than that of aprotic ILs and conventional organic solvents (4–8 V) [62–64]. This value is largely insensitive to trace water, as similar limits were observed under water-saturated conditions. Such restricted window is about 1 V narrower than standard type-III DESs such as ethaline and glyceline, but wider than ChCl:oxalic acid [19,65]. The measured ESW is comparable to that of menthol:acetic acid:ethanolamine on gold electrode [19], whereas an adequate comparison cannot be done with hydrophobic tetrabutylammonium chloride:decanoic acid measured by Ruggeri et al. [66], because their LSV were complicated by dissolved oxygen-reduction interference.

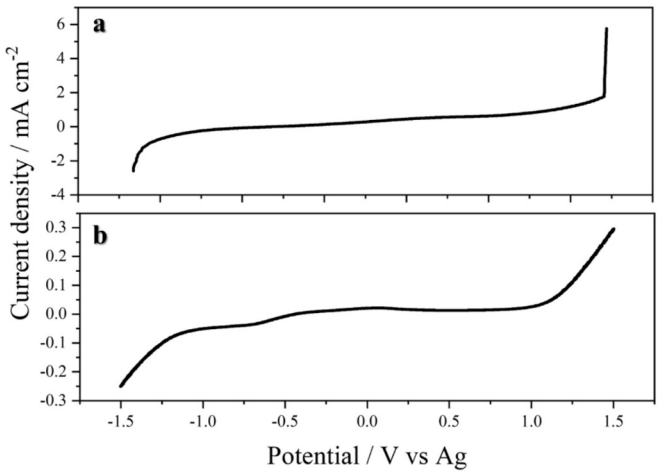

Fig. 6. LSV of a 10 wt% [HMIM][Cl] in Men:Dec (2:1) deep eutectic solvent on (a) gold electrode (b) stainless steel electrode. Electrode diameter: 0.5 mm. Ag wire was used as reference electrode and a graphite plate was used as counter electrode. All scans were performed at room temperature and at a sweep rate of 20 mV s^1.

The limited anodic stability could be attributed to the oxidation of menthol. The IL can also be involved in the oxidation and reduction processes delimiting the ESW. Imidazolium-based halides have a narrower ESW (eg. [HMIM][Cl] shows 3.2 V on Pt) because halides oxidize more readily than bulkier anions such as $[BF_4]^-$, $[PF_6]^-$ or $[Tf_2N]^-$ [67]. In addition, the easy removal of the acidic C_2—H of imidazolium facilitates reduction, thus narrowing the cathodic limit relative to other IL families. Further studies, for example with the aid of in situ surface-sensitive spectroscopic techniques, would help identify the species responsible for the ESW boundaries.

The ESW also depends on electrode material. Stainless steel shows reduced anodic stability, likely due to dissolution of surface oxides, but displays an extended cathodic range. This behavior is advantageous for electrochemically assisted metal-ion extraction using a cathodically polarized stainless-steel needle, as discussed later.

3.3.2. *Electrochemical behavior of the ferrocene/ferrocenium redox couple*

Ferrocene (Fc) oxidation to ferrocenium (Fc^+) is widely employed as a benchmark redox process in cyclic voltammetry (CV) and as an internal reference in organic media. Fc and several derivatives have been widely used to probe charge-transfer kinetics in various ILs and DESs on multiple electrode materials [19,46,66,68–73]. While many studies conducted in IL systems report diffusion-controlled, reversible Fc/Fc^+ behavior [46,69,70,72], others find quasi-reversible kinetics [71,74,75], depending on the Fc derivative, solvent, and electrode material. More recent studies conducted in both hydrophilic and hydrophobic DESs point to slower kinetics for the Fc/Fc^+ redox couple that shows quasi-reversible behavior [19,66,68].

Fig. 7a shows a representative CV for 2.7 mM Fc in the 10 wt% IL–NADES mixture (green line) alongside that for the background electrolyte (grey line). The Fc/Fc^+ couple exhibits well-defined anodic and cathodic peaks with a high faradaic-to-capacitive current ratio. Fig. 7b displays ohmic-drop-corrected CVs for scan rates from 5 to 250 mV·s^{-1}. Diagnostic parameters are summarized in Table 5. The voltammograms are symmetric around a half-wave potential ($E_{1/2}$) ≈ 0.306 V, which remains constant over the examined scan-rate range. Anodic and cathodic peak currents are comparable ($I_{p,c}$ / $I_{p,a}$ ≈ 1) at scan rates ≤100 mV·s^{-1}. At 250 mV·s^{-1}, ohmic distortion becomes significant despite resistance compensation. The peak-to-peak separation (ΔE_p) exceeds the ideal value of ~60 mV for a reversible one-electron process and increases with scan rate, confirming quasi-reversible electron transfer.

The heterogeneous standard rate constant, k^0, was estimated from the dimensionless kinetic parameter, $\Psi = k^0[RT/(nF\pi D\upsilon)]^{1/2}$, by using the well-known Nicholson approach, valid for ΔE_p < 212 mV [76]. In the equation above, D stands for the diffusion coefficient (cm^2 s^{-1}), υ is the scan rate (V s^{-1}), n is the number of transferred electrons, and the rest of symbols have their usual meaning and units. We applied the

Table 5
Data from the CV of 2.7 mM Fc in 10 wt% [HMIM][Cl]-NADES mixture at individual scan rates (from 5 to 250 mV s-1).

Scan rate (mV s^{-1})	E^c_p (V)[a]	E^a_p (V)[b]	I^c_p/I^a_p	ΔE_p (mV)	$E_{1/2}$ (V)	Ψ
5	0.2696	0.3462	1.11	76.6	0.3079	1.4368
10	0.2627	0.3473	1.15	84.6	0.3050	0.9761
20	0.2570	0.3542	1.07	97.2	0.3056	0.6481
50	0.2409	0.3634	1.09	122.5	0.3022	0.3868
100	0.2413	0.3781	1.08	136.8	0.3097	0.3150
250	0.2326	0.3805	n/a	147.9	0.3066	0.2754

[a] E^c_p is cathodic peak potential.
[b] E^a_p is anodic peak potential.

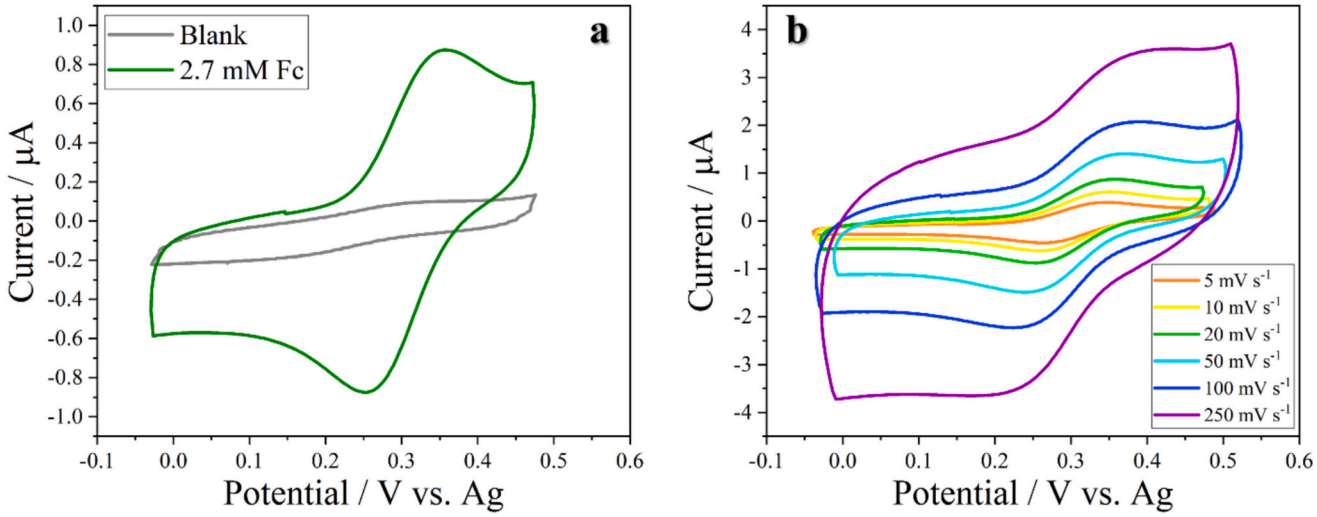

Fig. 7. Cyclic voltammograms in 10 wt% [HMIM][Cl]-NADES mixture. (a) Electrolyte background in abscence of Ferrocene (dark grey line) and representative CV in presence of 2.7 mM of Fc (dark green line) at 20 mV s^{-1}. (b) Ohmic-drop corrected cyclic voltammograms for Fc at different scan rates ranging from 5 to 250 mV s^{-1}. (For interpretation of the references to colour in this figure legend, the reader is referred to the web version of this article.)

empirical equation proposed by Lavagnini and coworkers [77] to obtain Ψ from experimentally determined ΔE_p at different scan rates (Table 5). The Ψ vs. $\upsilon^{-1/2}$ plot (Fig. S7) yields the slope from which k^0 can be obtained, provided the diffusion coefficient of Fc is known.

The diffusion coefficient of Fc was extracted from the variation of peak currents with scan rate, using corrected reversible peak currents $I_p = I_p^{rev} K(\Lambda, \alpha)$, where K is the Matsuda–Ayabe correction factor ($\Lambda = \Psi\sqrt{\pi}$) [78] and I_p is the average of experimental peak currents (Table S17). Assuming α = 0.5, calculated I_p^{rev} were plotted versus $\nu^1/^2$ (Fig. S8), and D was determined from the Randles–Ševčík equation ($I_p^{rev} = 269\, n^{3/2} D^{1/2} A C^* \upsilon^{1/2}$ at 25 °C). The resulting diffusion coefficient at 298 K is D = (6.16 ± 0.06) × 10^{-8} $cm^2 \cdot s^{-1}$. From this value, the standard rate constant for the Fc/Fc^+ quasi-reversible process is k^0 = (2.6 ± 0.3)·10^{-4} cm s^{-1}. The measured diffusivity agrees with values reported for Fc and its derivatives in typical RTILs [46,69,70,72], hydrophilic DESs [68,73] and hydrophobic DESs [19] of similar viscosity (10^{-7}–10^{-8} cm^2 s^{-1}). The obtained k^0 is comparable to those found in quaternary ammonium and phosphonium salt DESs [68], but about one order of magnitude slower than in most imidazolium ILs [70,74,75] and slower still than in conventional organic solvents [79,80]. The result is also consistent with reported k^0 values (10^{-5}–10^{-4} cm s^{-1}) for choline chloride-based DESs [68,81], although wider discrepancies exist in the literature due to variations in electrode materials, solvent compositions and applied experimental conditions [80,82]. A comparison of our Fc standard rate constant with literature data can be found in Table S18.

3.4. Potential applicability of eutectic mixture

After evaluating the physicochemical properties and electrochemical behavior of the eutectic mixture formed by a menthol-based DES and HMIMCl, its usefulness as an extractant in electro-assisted microextraction application was tested and compared to conventional microextraction.

For this purpose, two sets of microextraction experiments (three replicates each) were carried out under the same stirring conditions, extraction time, pH, chelating agent and metal concentrations in the aqueous sample phase (400 μg kg^{-1} of Cd, Cr, Ni, Pb, and Zn in cationic form), with the only difference being the application or not of a cathodic potential (−0.75 V vs Ag) to the working electrode needle. Fig. 8 compares the ICP-OES signals obtained for the conventional microextraction operation (grey bars) and those corresponding to the electrochemically controlled extraction (green bars). Up to an 8-fold gain in the recorded ICP-OES signal was obtained with respect to the non-stimulated microextraction. Our results provide clear evidence that the application of the electrochemically controlled methodology gives rise to a significant enhancement of the extraction of all the metal ions investigated.

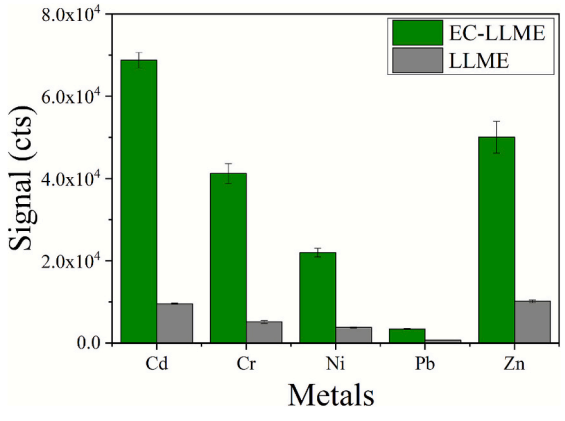

Fig. 8. ICP-OES signals after electrochemically controlled (EC-LLME, green bars) and conventional (LLME, grey bars) liquid-liquid microextraction of metals. Sample concentration: 400 μg kg^{-1}, extraction time: 5 min, [8-HQ]: 1 %, sample volume: 10 mL, sample pH: 4.66, NADES volume: 315 μL, applied potential to EC-LLME: −0.75 V vs Ag. The error bars correspond to the standard deviation of 3 replicates. (For interpretation of the references to colour in this figure legend, the reader is referred to the web version of this article.)

It can thus be concluded that the menthol-based eutectic mixture studied has the potential for use in electrochemical applications, with electrochemically controlled liquid-liquid microextraction representing one of the most innovative and viable avenues for its deployment.

4. Conclusions

A hydrophobic NADES based on DL-menthol and decanoic acid (2:1) was combined with up to 50 wt% [HMIM][Cl] to generate eutectic mixtures with tunable conductivity, viscosity, and density. The added IL enhances ionic conductivity while preserving the desirable low viscosity and hydrophobicity of the parent solvent. Both conductivity and viscosity follow Arrhenius-type behavior. Positive excess molar volumes and negative viscosity deviations suggest the formation of a less efficiently packed medium with a partially reorganized hydrogen-bond network and weakened IL ion–ion interactions. These conclusions are supported by IR spectral shifts associated with hydrogen-bond-sensitive vibrational modes.

Walden analysis shows that the eutectic mixtures behave as low-ionicity liquids, although ionicity increases with IL content. This trend is corroborated by the rise in molar conductivity and the calculated increase in the degree of ion dissociation. The behavior is attributed to the "re-dissociation" of neutral ion pairs into larger charged aggregates (e.g., ion triplets), as commonly observed for ILs dissolved in low-permittivity organic solvents.

The most dilute [HMIM][Cl]–NADES mixture displays an electrochemical stability window of approximately 2.5 V. Cyclic voltammetry reveals quasi-reversible electron-transfer kinetics of the ferrocene redox probe, with a standard rate constant $k^0 = (2.6 \pm 0.3)\cdot 10^{-4}$ cm s^{-1}, and a diffusion coefficient $D = (6.16 \pm 0.06)\cdot 10^{-8}$ cm^2 s^{-1}, values comparable to those reported for other DESs of similar viscosity.

The successful application of the IL–NADES mixture in an electrochemically assisted liquid–liquid microextraction (EC-LLME) method—significantly enhancing heavy-metal extraction from aqueous samples—demonstrates its analytical utility. The low toxicity, low viscous and moderately conductive menthol-based eutectic mixture holds considerable promise for sustainable applications in electrochemistry, and analytical separations, paving the way for its use in areas such as electrochemical sensing and environmentally friendly extraction processes.

Declaration of generative AI in scientific writing

During the preparation of this work, the authors used ChatGPT-4 to assist with text processing, translation, English language correction, and improving readability. After using this service, the authors reviewed and edited the content as needed and took full responsibility for the content of the published article.

CRediT authorship contribution statement

Andrea Marco: Writing – original draft, Visualization, Validation, Methodology, Investigation, Formal analysis, Data curation, Conceptualization. **César Quijada:** Writing – review & editing, Visualization, Supervision, Funding acquisition, Formal analysis, Data curation, Conceptualization. **Miguel Ángel Aguirre:** Writing – review & editing, Supervision, Methodology, Investigation, Funding acquisition, Conceptualization. **Montserrat Hidalgo:** Writing – review & editing, Supervision, Project administration, Funding acquisition, Conceptualization.

Declaration of competing interest

The authors declare that they have no known competing financial interests or personal relationships that could have appeared to influence the work reported in this paper.

Acknowledgements

The authors are grateful for the financial support received from the Valencia Regional Government (Spain) (CIPROM/2021/062) and the Spanish Ministry of Science and Innovation (PID2021-126155OB-I00). Authors also wish to thank the Spanish Network of Excellence in Sample Preparation (RED2022-134079-T), which was granted by the Spanish Ministry of Science and Innovation, and the Sample Preparation Study Group and Network, which were sponsored by the European Chemical Society's Division of Analytical Chemistry. Funding for open access charges from CRUE-Universitat Politècnica de València is gratefully acknowledged.

Appendix A. Supplementary data

Supplementary data to this article can be found online at https://doi.org/10.1016/j.molliq.2025.129173.

Data availability

Data will be made available on request.

References

[1] C.J. Clarke, W.C. Tu, O. Levers, A. Bröhl, J.P. Hallett, Green and sustainable solvents in chemical processes, Chem. Rev. 118 (2018) 747–800, https://doi.org/10.1021/acs.chemrev.7b00571.
[2] E.L. Smith, A.P. Abbott, K.S. Ryder, Deep eutectic solvents (DESs) and their applications, Chem. Rev. 114 (2014) 11060–11082, https://doi.org/10.1021/cr300162p.
[3] B.B. Hansen, S. Spittle, B. Chen, D. Poe, Y. Zhang, J.M. Klein, A. Horton, L. Adhikari, T. Zelovich, B.W. Doherty, B. Gurkan, E.J. Maginn, A. Ragauskas, M. Dadmun, T.A. Zawodzinski, G.A. Baker, M.E. Tuckerman, R.F. Savinell, J. R. Sangoro, Deep eutectic solvents: a review of fundamentals and applications, Chem. Rev. 121 (2021) 1232–1285, https://doi.org/10.1021/acs.chemrev.0c00385.
[4] J. Wu, Q. Liang, X. Yu, L. Qiu-Feng, L. Ma, X. Qin, G. Chen, B. Li, Deep eutectic solvents for boosting electrochemical energy storage and conversion: a review and perspective, Adv. Funct. Mater. 31 (2021) 2011102, https://doi.org/10.1002/adfm.202011102.
[5] F. Endres, D. Macfarlane, A. Abbott, Electrodeposition from Ionic Liquids, 2nd ed., Wiley-VCH Verlag GmbH&Co, Weinheim, Germany, 2017.
[6] B.D. Ribeiro, C. Florindo, L.C. Iff, M.A.Z. Coelho, I.M. Marrucho, Menthol-based eutectic mixtures: hydrophobic low viscosity solvents, ACS Sustain. Chem. Eng. 3 (2015) 2469–2477, https://doi.org/10.1021/acssuschemeng.5b00532.
[7] D.J.G.P. Van Osch, C.H.J.T. Dietz, S.E.E. Warrag, M.C. Kroon, The curious case of hydrophobic deep eutectic solvents: a story on the discovery Design, and Applications, ACS Sustain. Chem. Eng. 8 (2020) 10591–10612, https://doi.org/10.1021/acssuschemeng.0c00559.
[8] D.O. Abranches, M.A.R. Martins, L.P. Silva, N. Schaeffer, S.P. Pinho, J.A. P. Coutinho, Phenolic hydrogen bond donors in the formation of non-ionic deep eutectic solvents: the quest for type v des, Chem. Commun. 55 (2019) 10253–10256, https://doi.org/10.1039/c9cc04846d.
[9] M. Cherniakova, V. Varchenko, K. Belikov, Menthol-based (deep) eutectic solvents: a review on properties and application in extraction, Chem. Rec. 24 (2024) e202300267, https://doi.org/10.1002/tcr.202300267.
[10] F. Bergua, M. Castro, J. Muñoz-Embid, C. Lafuente, M. Artal, L-menthol-based eutectic solvents: characterization and application in the removal of drugs from water, J. Mol. Liq. 352 (2022) 118754, https://doi.org/10.1016/j.molliq.2022.118754.
[11] F.C. Pinheiro, M.Á. Aguirre, J.A. Nóbrega, N. González-Gallardo, D.J. Ramón, A. Canals, Dispersive liquid-liquid microextraction based on deep eutectic solvent for elemental impurities determination in oral and parenteral drugs by inductively coupled plasma optical emission spectrometry, Anal. Chim. Acta 1185 (2021) 339052, https://doi.org/10.1016/j.aca.2021.339052.
[12] S. Nojavan, H. Shaghaghi, T. Rahmani, A. Shokri, M. Nasiri-Aghdam, Combination of electromembrane extraction and electro-assisted liquid-liquid microextraction: a tandem sample preparation method, J. Chromatogr. A 1563 (2018) 20–27, https://doi.org/10.1016/j.chroma.2018.05.068.
[13] S. Liu, Y. Huang, C. Qian, Z. Xiang, G. Ouyang, Physical assistive technologies of solid-phase microextraction: recent trends and future perspectives, TrAC - Trends in Analytical Chemistry 128 (2020) 115916, https://doi.org/10.1016/j.trac.2020.115916.
[14] Q. Li, Y. Ding, D. Yuan, Electrosorption-enhanced solid-phase microextraction of trace anions using a platinum plate coated with single-walled carbon nanotubes, Talanta 85 (2011) 1148–1153, https://doi.org/10.1016/j.talanta.2011.05.042.
[15] J. Qiu, F. Wang, T. Zhang, L. Chen, Y. Liu, F. Zhu, G. Ouyang, Novel Electrosorption-enhanced solid-phase microextraction device for ultrafast in vivo sampling of ionized Pharmaceuticals in Fish, Environ. Sci. Technol. 52 (2018) 145–151, https://doi.org/10.1021/acs.est.7b04883.
[16] H. Sereshti, F. Karami, N. Nouri, A. Farahani, Electrochemically controlled solid phase microextraction based on a conductive polyaniline-graphene oxide nanocomposite for extraction of tetracyclines in milk and water, J. Sci. Food Agric. 101 (2021) 2304–2311, https://doi.org/10.1002/jsfa.10851.
[17] H. Asiabi, Y. Yamini, M. Shamsayei, J.A. Mehraban, A nanocomposite prepared from a polypyrrole deep eutectic solvent and coated onto the inner surface of a steel capillary for electrochemically controlled microextraction of acidic drugs such as losartan, Microchim. Acta 185 (2018) 169, https://doi.org/10.1007/s00604-018-2684-y.
[18] S. Anjali, Pandey, ethanolamine-mediated microstructural transitions within terpenoid- and fatty acid-based deep eutectic solvents, Phys. Chem. Chem. Phys. 27 (2025) 3124–3137, https://doi.org/10.1039/D4CP03878A.
[19] N. Chaabene, K. Ngo, M. Turmine, V. Vivier, New hydrophobic deep eutectic solvent for electrochemical applications, J. Mol. Liq. 319 (2020) 114198, https://doi.org/10.1016/j.molliq.2020.114198.
[20] J. Zhao, J. Zhang, W. Yang, B. Chen, Z. Zhao, H. Qiu, S. Dong, X. Zhou, G. Cui, L. Chen, "Water-in-deep eutectic solvent" electrolytes enable zinc metal anodes for rechargeable aqueous batteries, Nano Energy 57 (2019) 625–634, https://doi.org/10.1016/j.nanoen.2018.12.086.
[21] N.F. Gajardo-Parra, M.J. Lubben, J.M. Winnert, Á. Leiva, J.F. Brennecke, R. I. Canales, Physicochemical properties of choline chloride-based deep eutectic solvents and excess properties of their pseudo-binary mixtures with 1-butanol, J. Chem. Thermodyn. 133 (2019) 272–284, https://doi.org/10.1016/j.jct.2019.02.010.
[22] V. Agieienko, R. Buchner, A comprehensive study of density, viscosity, and electrical conductivity of (choline chloride + glycerol) deep eutectic solvent and its mixtures with dimethyl sulfoxide, J. Chem. Eng. Data 66 (2021) 780–792, https://doi.org/10.1021/acs.jced.0c00869.
[23] R.S. Achsah, S. Shyam, N. Mayuri, R. Anantharaj, Thermodynamic Properties of Deep Eutectic Solvent and Ionic Liquid Mixtures at Temperatures from 293.15 K to 343.15 K, AIP Conf Proc, American Institute of Physics Inc., in, 2018, https://doi.org/10.1063/1.5031718.
[24] H. Shekaari, M. Taghi Zafarani-Moattar, M. Mokhtarpour, S. Faraji, Compatibility of sustainable solvents ionic liquid, 1-ethyl-3-methylimidazolium ethyl sulfate in some choline chloride based deep eutectic solvents: thermodynamics study, J. Chem. Thermodyn. 141 (2020) 105961, https://doi.org/10.1016/j.jct.2019.105961.
[25] J. Panić, S. Papović, B. Šarac, R. Cerc Korošec, M. Rapaić, S. Gadžurić, M. Bešter-Rogač, M. Vraneš, Active pharmaceutical ingredient ionic liquid in natural deep eutectic solvents – influence of solvent composition, J. Mol. Liq. 384 (2023) 122282, https://doi.org/10.1016/j.molliq.2023.122282.
[26] K.K. de L. Augusto, G.R. Piton, P.C. Gomes-Júnior, G.P. Longatto, F.C. de Moraes, O. Fatibello-Filho, Enhancing the electrochemical sensitivity of hydroquinone using a hydrophobic deep eutectic solvent-based carbon paste electrode, Anal. Methods 14 (2022) 2003–2013, https://doi.org/10.1039/d2ay00473a.
[27] N. Wannasri, P. Uppachai, K. Seehamart, S. Jantrasee, N. Butwong, K. Mukdasai, I. M. Isa, S. Mukdasai, Novel and highly sensitive electrochemical sensor for the determination of oxytetracycline based on fluorine-doped activated carbon and hydrophobic deep eutectic solvents, ACS Omega 7 (2022) 45654–45664, https://doi.org/10.1021/acsomega.2c06462.
[28] M.E. Di Pietro, A. Mele, Deep eutectics and analogues as electrolytes in batteries, J. Mol. Liq. 338 (2021) 116597, https://doi.org/10.1016/j.molliq.2021.116597.
[29] D.J.G.P. Van Osch, C.H.J.T. Dietz, J. Van Spronsen, M.C. Kroon, F. Gallucci, M. Van Sint Annaland, R. Tuinier, A search for natural hydrophobic deep eutectic solvents based on natural components, ACS Sustain. Chem. Eng. 7 (2019) 2933–2942, https://doi.org/10.1021/acssuschemeng.8b03520.
[30] C. Quijada, F.J. Huerta, E. Morallón, J.L. Vázquez, L.E.A. Berlouis, Electrochemical behaviour of aqueous SO_2 at polycrystalline gold electrodes in acidic media: a voltammetric and in situ vibrational study Part 1. Reduction of SO_2 : deposition of monomeric and polymeric sulphur, Electrochim. Acta 45 (2000) 1847–1862, https://doi.org/10.1016/S0013-4686(99)00396-5.
[31] Y. Saito, J.J. Wang, D.N. Batchelder, D.A. Smith, Simple chemical method for forming silver surfaces with controlled grain sizes for surface plasmon experiments, Langmuir 19 (2003) 6857–6861, https://doi.org/10.1021/la0301240.
[32] A. Marco, M.Á. Aguirre, C. Quijada, M. Hidalgo, Electrochemically controlled liquid-liquid microextraction: an innovative methodology for heavy metal extraction from tea using non-toxic menthol-based eutectic mixture, Anal. Chim. Acta 1375 (2025) 344542, https://doi.org/10.1016/j.aca.2025.344542.
[33] H. Ning, M.Q. Hou, Q.Q. Mei, Y.H. Liu, D.Z. Yang, B.X. Han, The physicochemical properties of some imidazolium-based ionic liquids and their binary mixtures, Sci. China Chem. 55 (2012) 1509–1518, https://doi.org/10.1007/s11426-012-4655-1.
[34] W. Zhang, X. Chen, Y. Wang, L. Wu, Y. Hu, Experimental and modeling of conductivity for electrolyte solution systems, ACS Omega 5 (2020) 22465–22474, https://doi.org/10.1021/acsomega.0c03013.
[35] H. Wang, Z. Zuo, L. Lu, A. Laaksonen, Y. Wang, X. Lu, X. Ji, Experimental and theoretical study on ion association in [Hmim][halide] + water/isopropanol

mixtures, Fluid Phase Equilib. 566 (2023) 113680, https://doi.org/10.1016/j.fluid.2022.113680.
[36] F. Ahmed, D. Paterno, G. Singh, S. Suarez, Ion transport in non-aqueous electrolyte mixtures of zinc chloride deep eutectic solvent (DES) and molecular solvents, Electrochim. Acta 462 (2023) 142784, https://doi.org/10.1016/j.electacta.2023.142784.
[37] R. Kenneth, Seddon, Annegret Stark, María-José Torres, Viscosity and density of 1-alkyl-3-methylimidazolium Ionic Liquids in Clean solvents alternative media for chemical reactions and processing, ACS Symp. Ser. 819 (2002) 34–49, https://doi.org/10.1021/bk-2002-0819.ch004. Chapter 4.
[38] E.J. González, M. González-Miquel, I. Díaz, M. Rodríguez, C. Fontela, R. Cañadas, J. Sánchez, Enhancing aqueous systems fermentability using hydrophobic eutectic solvents as extractans of inhibitory compounds, Sep. Purif. Technol. 250 (2020) 117184, https://doi.org/10.1016/j.seppur.2020.117184.
[39] F. Li, Z. Zuo, B. Cao, X. Ji, Study on the thermodynamic properties of ionic liquids 1-Hexyl-3-methylimidazolium halide with isopropanol mixtures, J. Chem. Eng. Data (2024) 3794–3804, https://doi.org/10.1021/acs.jced.4c00343.
[40] Y. Yang, J. Zhao, R. Zhao, H. Lin, S. Xu, Y. Zhou, Study of the intermolecular interaction in hydrophobic deep eutectic solvent of (2-n-octyl-4-isothiazolin-3-one + 1-decanol) from the density, viscosity, thermodynamic, spectroscopic and quantum chemical calculations, J. Chem. Thermodyn. 195 (2024) 107302, https://doi.org/10.1016/j.jct.2024.107302.
[41] E. Gómez, B. González, Á. Domínguez, E. Tojo, J. Tojo, Dynamic viscosities of a series of 1-alkyl-3-methylimidazolium chloride ionic liquids and their binary mixtures with water at several temperatures, J. Chem. Eng. Data 51 (2006) 696–701, https://doi.org/10.1021/je050460d.
[42] F. Kermanpour, M.M. Rabie, S. Broumand, A thermodynamic and physical study on (1-Hexyl-3-methylimidazolium chloride + 1-pentanol and ethylene glycol) binary mixtures at temperatures (293.15–333.15) K, J. Solut. Chem. 46 (2017) 2091–2108, https://doi.org/10.1007/s10953-017-0695-7.
[43] F. Yang, Q. Ma, X. Wang, Z. Liu, Effect of organic solvents on lowering the viscosity of 1-hexyl-3-methylimidazolium chloride, J. Chem. Thermodyn. 113 (2017) 358–368, https://doi.org/10.1016/j.jct.2017.07.016.
[44] C. Schreiner, S. Zugmann, R. Hartl, H.J. Gores, Temperature dependence of viscosity and specific conductivity of fluoroborate-based ionic liquids in light of the fractional Walden rule and Angell's fragility concept, J. Chem. Eng. Data 55 (2010) 4372–4377, https://doi.org/10.1021/je1005505.
[45] C. Austen Angell, Y. Ansari, Z. Zhao, Ionic Liquids: Past, present and future, Faraday Discuss. 154 (2012) 9–27, https://doi.org/10.1039/c1fd00112d.
[46] R. Khalil, N. Chaabene, M. Azar, I.B. Malham, M. Turmine, Effect of the chain lengthening on transport properties of imidazolium-based ionic liquids, Fluid Phase Equilib. 503 (2020) 112316, https://doi.org/10.1016/j.fluid.2019.112316.
[47] S. Azmi, M.F. Koudahi, E. Frackowiak, Reline deep eutectic solvent as a green electrolyte for electrochemical energy storage applications, Energy Environ. Sci. 15 (2022) 1156–1171, https://doi.org/10.1039/d1ee02920g.
[48] O. Nordness, J.F. Brennecke, Ion dissociation in ionic liquids and ionic liquid solutions, Chem. Rev. 120 (2020) 12873–12902, https://doi.org/10.1021/acs.chemrev.0c00373.
[49] J. Hunger, A. Stoppa, R. Buchner, G. Hefter, From ionic liquid to electrolyte solution: dynamics of 1-n-butyl-3-N- methylimidazolium tetrafluoroborate/dichloromethane mixtures, J. Phys. Chem. B 112 (2008) 12913–12919, https://doi.org/10.1021/jp8045627.
[50] N.T. Scharf, A. Stark, M.M. Hoffmann, Ion pairing and dynamics of the ionic liquid 1-hexyl-3-methylimidazolium bis(irifluoromethylsulfonyl)amide ([C_6mim][NTf_2]) in the low dielectric solvent chloroform, J. Phys. Chem. B 116 (2012) 11488–11497, https://doi.org/10.1021/jp3047592.
[51] O. Nordness, L.D. Simoni, M.A. Stadtherr, J.F. Brennecke, Characterization of aqueous 1-Ethyl-3-methylimidazolium ionic liquids for calculation of ion dissociation, J. Phys. Chem. B 123 (2019) 1348–1358, https://doi.org/10.1021/acs.jpcb.8b11892.
[52] K. Hayamizu, Y. Aihara, H. Nakagawa, T. Nukuda, W.S. Price, Ionic conduction and ion diffusion in binary room-temperature ionic liquids composed of [emim][BF_4] and $LiBF_4$, J. Phys. Chem. B 108 (2004) 19527–19532, https://doi.org/10.1021/jp0476601.
[53] S. Katsuta, K. Imai, Y. Kudo, Y. Takeda, H. Seki, M. Nakakoshi, Ion pair formation of alkylimidazolium ionic liquids in dichloromethane, J. Chem. Eng. Data 53 (2008) 1528–1532, https://doi.org/10.1021/je800152d.
[54] K.R. Ramya, P. Kumar, A. Venkatnathan, Molecular simulations of anion and temperature dependence on structure and dynamics of 1-Hexyl-3-methylimidazolium ionic liquids, J. Phys. Chem. B 119 (2015) 14800–14806, https://doi.org/10.1021/acs.jpcb.5b09456.
[55] H. Tokuda, K. Hayamizu, K. Ishii, M.A.B.H. Susan, M. Watanabe, Physicochemical properties and structures of room temperature ionic liquids. 2. Variation of alkyl chain length in imidazolium cation, J. Phys. Chem. B 109 (2005) 6103–6110, https://doi.org/10.1021/jp044626d.
[56] D.R. Saeva, J. Petenuci, M.M. Hoffmann, Transport properties of the 1-Hexyl-3-methylimidazolium bis(trifluoromethylsulfonyl)amide-trichloromethane binary system: indication of trichloromethane segregation, J. Phys. Chem. B 120 (2016) 9745–9754, https://doi.org/10.1021/acs.jpcb.6b06974.
[57] Y. Na, X. Gao, J. Hong, X. Zhou, N. Liang, L. Zhao, Vortex-assisted dispersive liquid–liquid microextraction based on the hydrophobic deep eutectic solvent–based ferrofluid for extraction and detection of myclobutanil, Microchim. Acta 190 (2023) 352, https://doi.org/10.1007/s00604-023-05884-y.
[58] V.H. Paschoal, L.F.O. Faria, M.C.C. Ribeiro, Vibrational spectroscopy of ionic liquids, Chem. Rev. 117 (2017) 7053–7112, https://doi.org/10.1021/acs.chemrev.6b00461.
[59] T. Yamada, Y. Tominari, S. Tanaka, M. Mizuno, Infrared spectroscopy of ionic liquids consisting of imidazolium cations with different alkyl chain lengths and various halogen or molecular anions with and without a small amount of water, J. Phys. Chem. B 121 (2017) 3121–3129, https://doi.org/10.1021/acs.jpcb.7b01429.
[60] Z. Ren, X. Wu, H. Yu, F. Zhang, S. Tian, Z. Zhou, Effective separation of toluene from n-heptane with imidazolium-based deep eutectic solvents, Fuel 326 (2022) 124992, https://doi.org/10.1016/j.fuel.2022.124992.
[61] X. Wu, J.J. Shi, H. Yu, Q. Li, Z. Zhou, Z. Ren, Pyridine ionic liquid-based deep eutectic solvents selectively separating toluene from alkanes, Energy Fuel 37 (2023) 4233–4243, https://doi.org/10.1021/acs.energyfuels.2c03681.
[62] M. Galiński, A. Lewandowski, I. Stepniak, Ionic liquids as electrolytes, Electrochim. Acta 51 (2006) 5567–5580, https://doi.org/10.1016/j.electacta.2006.03.016.
[63] W. Adamiak, D. Kałuża, M. Jönsson-Niedziolka, Compatibility of organic solvents for electrochemical measurements in PDMS-based microfluidic devices, Microfluid. Nanofluid. 20 (2016) 127, https://doi.org/10.1007/s10404-016-1792-4.
[64] K. Gong, Q. Fang, S. Gu, S.F.Y. Li, Y. Yan, Nonaqueous redox-flow batteries: organic solvents, supporting electrolytes, and redox pairs, energy, Environ. Sci. 8 (2015) 3515–3530, https://doi.org/10.1039/c5ee02341f.
[65] Q. Li, J. Jiang, G. Li, W. Zhao, X. Zhao, T. Mu, The electrochemical stability of ionic liquids and deep eutectic solvents, Sci. China Chem. 59 (2016) 571–577, https://doi.org/10.1007/s11426-016-5566-3.
[66] S. Ruggeri, F. Poletti, C. Zanardi, L. Pigani, B. Zanfrognini, E. Corsi, N. Dossi, M. Salomäki, H. Kivelä, J. Lukkari, F. Terzi, Chemical and electrochemical properties of a hydrophobic deep eutectic solvent, Electrochim. Acta 295 (2019) 124–129, https://doi.org/10.1016/j.electacta.2018.10.086.
[67] L.E. Barrosse-Antle, A.M. Bond, R.G. Compton, A.M. O'Mahony, E.I. Rogers, D. S. Silvester, Voltammetry in room temperature ionic liquids: comparisons and contrasts with conventional electrochemical solvents, Chem. Asian J. 5 (2010) 202–230, https://doi.org/10.1002/asia.200900191.
[68] L. Bahadori, N.S. Abdul Manan, M.H. Chakrabarti, M.A. Hashim, F.S. Mjalli, I. M. Alnashef, M.A. Hussain, C.T.J. Low, The electrochemical behaviour of ferrocene in deep eutectic solvents based on quaternary ammonium and phosphonium salts, Phys. Chem. Chem. Phys. 15 (2013) 1707–1714, https://doi.org/10.1039/c2cp43077k.
[69] A.W. Taylor, P. Licence, A.P. Abbott, Non-classical diffusion in ionic liquids, Phys. Chem. Chem. Phys. 13 (2011) 10147–10154, https://doi.org/10.1039/c1cp20373h.
[70] C.L. Bentley, J. Li, A.M. Bond, J. Zhang, Mass-transport and heterogeneous electron-transfer kinetics associated with the ferrocene/ferrocenium process in ionic liquids, J. Phys. Chem. C 120 (2016) 16516–16525, https://doi.org/10.1021/acs.jpcc.6b05545.
[71] N. Frenzel, J. Hartley, G. Frisch, Voltammetric and spectroscopic study of ferrocene and hexacyanoferrate and the suitability of their redox couples as internal standards in ionic liquids, Phys. Chem. Chem. Phys. 19 (2017) 28841–28852, https://doi.org/10.1039/c7cp05483a.
[72] M. Thakurathi, E. Gurung, M.M. Cetin, V.D. Thalangamaarachchige, M.F. Mayer, C. Korzeniewski, E.L. Quitevis, The stokes-einstein equation and the diffusion of ferrocene in imidazolium-based ionic liquids studied by cyclic voltammetry: effects of cation ion symmetry and alkyl chain length, Electrochim. Acta 259 (2018) 245–252, https://doi.org/10.1016/j.electacta.2017.10.149.
[73] S. Fryars, E. Limanton, F. Gauffre, L. Paquin, C. Lagrost, P. Hapiot, Diffusion of redox active molecules in deep eutectic solvents, J. Electroanal. Chem. 819 (2018) 214–219, https://doi.org/10.1016/j.jelechem.2017.10.030.
[74] D.Y. Kim, J.C. Yang, H.W. Kim, G.M. Swain, Heterogeneous electron-transfer rate constants for ferrocene and ferrocene carboxylic acid at boron-doped diamond electrodes in a room temperature ionic liquid, Electrochim. Acta 94 (2013) 49–56, https://doi.org/10.1016/j.electacta.2013.01.140.
[75] A.S. Barnes, E.I. Rogers, I. Streeter, L. Aldous, C. Hardacre, R.G. Compton, Extraction of electrode kinetic parameters from microdisc voltammetric data measured under transport conditions intermediate between steady-state convergent and transient linear diffusion as typically applies to room temperature ionic liquids, J. Phys. Chem. B 112 (2008) 7560–7565, https://doi.org/10.1021/jp711897b.
[76] R.S. Nicholson, Theory and application of cyclic voltammetry for measurement of electrode reaction kinetics, Anal. Chem. 37 (1965) 1351–1355.
[77] I. Lavagnini, R. Antiochia, F. Magno, An extended method for the practical evaluation of the standard rate constant from cyclic voltammetric data, Electroanalysis 16 (2004) 505–506, https://doi.org/10.1002/elan.200302851.
[78] H. Matsuda, Y. Ayabe, Zur Theorie der Randles-Sevčikschen Kathodenstrahl-Polarographie, Z. Elektrochem. 59 (1955) 494–503.
[79] N.G. Tsierkezos, U. Ritter, Electrochemical impedance spectroscopy and cyclic voltammetry of ferrocene in acetonitrile/acetone system, J. Appl. Electrochem. 40 (2010) 409–417, https://doi.org/10.1007/s10800-009-0011-3.
[80] F. Zhen, L. Percevault, L. Paquin, E. Limanton, C. Lagrost, P. Hapiot, Electron transfer kinetics in a deep eutectic solvent, J. Phys. Chem. B 124 (2020) 1025–1032, https://doi.org/10.1021/acs.jpcb.9b09022.
[81] L. Bahadori, M.H. Chakrabarti, F.S. Mjalli, I.M. Alnashef, N.S.A. Manan, M. A. Hashim, Physicochemical properties of ammonium-based deep eutectic solvents and their electrochemical evaluation using organometallic reference redox systems, Electrochim. Acta 113 (2013) 205–211, https://doi.org/10.1016/j.electacta.2013.09.102.
[82] C.A. Nkuku, R.J. LeSuer, Electrochemistry in deep eutectic solvents, J. Phys. Chem. B 111 (2007) 13271–13277, https://doi.org/10.1021/jp075794j.